DMD Fast Forward. Published on July 28, 2021 as DOI: 10.1124/dmd.120.000234
This article has not been copyedited and formatted. The final version may differ from this version.

Title: Preclinical Drug Metabolism, Pharmacokinetic, and Pharmacodynamic Profiles of Ivosidenib, an Inhibitor of Mutant IDH1 for Treatment of *IDH1*-Mutant Malignancies

Authors: Yue Chen, Nelamangala V. Nagaraja, Bin Fan, Luke Utley, Rene M. Lemieux, Janeta Popovici-Muller, Lenny Dang, Hyeryun Kim, Liping Yan, Shin-San M. Su, Scott A. Biller, and Hua Yang

Affiliations at time of manuscript submission: *Agios Pharmaceuticals, Inc., Cambridge, Massachusetts (Y.C., N.V.N., B.F., L.U., R.M.L., J.P.-M., L.D., H.K., S.-S.M.S., S.A.B., H.Y.); and ChemPartner, Shanghai 201203, China (L.Y.)*

Current affiliations:

Servier Pharmaceuticals LLC, Boston, Massachusetts (N.V.N.); KLUS Pharma, Cranbury, New Jersey (B.F.); Ribon Therapeutics, Cambridge, Massachusetts (L.U.); Faze Medicines, Inc., Cambridge, Massachusetts (R.M.L.); Rectify Pharmaceuticals, Cambridge, Massachusetts (J.P.-M.); Volastra Therapeutics, Inc., New York, New York (S.-S.M.S.); and Disc Medicine, Cambridge, Massachusetts (H.Y.)

Running title: Preclinical Drug Metabolism and PK Profile of Ivosidenib

Address correspondence to: Nelamangala V. Nagaraja, Servier Pharmaceuticals LLC, 200
Pier Four Boulevard, Boston, MA 02210, USA. E-mail:
raj.nagaraja@servier.com; Tel: 857-262-3525; Fax: 800-807-9103

Text Pages: 31

Tables: 8

Figures: 4

References: 29

Abstract: 228 words

Introduction: 490 words

Discussion: 1497 words

ABBREVIATIONS: 2-HG, D-2-hydroxyglutarate; AML, acute myeloid leukemia; $AUC_{0–12h}$, area under the concentration-time curve from time 0 to 12 hours postdose; $AUC_{0–24h}$, area under the concentration-time curve from time 0 to 24 hours postdose; $AUC_{0–inf}$, area under the concentration-time curve extrapolated to infinity; BCRP, breast cancer resistance protein; CL, clearance; CL_{hep}, hepatic clearance; CL_{int}, intrinsic clearance; CL_r, renal clearance; C_{max}, maximum plasma concentration; CSF, cerebrospinal fluid; C_{trough}, trough concentration; CYP, cytochrome P450; DMSO, dimethyl sulfoxide; E0, baseline effect, corresponding to response when dose of drug is zero; EAUC, efficacious area under the curve; $EAUC_{50/90/97}$(0–12h), EAUC from 0–12h resulting in 50/90/97% tumor 2-HG inhibition; EC_{50}, half-maximal effective concentration; Eh, hepatic extraction ratio; E_{max}, maximum effect; F, bioavailability; FDA, US Food and Drug Administration; f_u, fraction unbound; f_{ut}, fraction unbound in tissues; i.v., intravenous; IDH, isocitrate dehydrogenase; LC-MS/MS, liquid chromatography with tandem mass spectrometry; MDCKII, Madin-Darby Canine Kidney II; mIDH, mutant isocitrate dehydrogenase; NA, not applicable; NADPH, nicotinamide adenine dinucleotide phosphate; NC, not calculated; NT, not tested; P_{app}, apparent permeability; PD, pharmacodynamic; P-gp, P-glycoprotein; PK, pharmacokinetic; q.d., once daily; Q_H, liver blood flow; $R_{e/i}$, ratio of total protein in extracellular fluid outside plasma to total protein in plasma; $t_{½}$, half-life; T_{max}, time to maximum concentration; V_e, extracellular volume minus plasma volume; V_r, volume into which drug distributes minus extracellular space; V_{ss}, volume of distribution at a steady state.

Abstract

Point mutations in isocitrate dehydrogenase 1 (*IDH1*) result in conversion of α-ketoglutarate to the oncometabolite, D-2-hydroxyglutarate (2-HG). Ivosidenib is a once daily (q.d.), orally available, potent, mutant IDH1 (mIDH1) inhibitor approved for the treatment of patients with relapsed or refractory acute myeloid leukemia (AML) and intensive chemotherapy-ineligible newly diagnosed AML, with a susceptible *IDH1* mutation. We characterized the protein binding, metabolism, metabolites, cell permeability, and drug-drug interaction potential of ivosidenib in humans, monkeys, dogs, rats, and/or mice in in vitro experiments. In vivo pharmacokinetic (PK) profiling and assessment of drug distribution and excretion was undertaken in rats, dogs, and monkeys administered single-dose ivosidenib. The PK/pharmacodynamic (PD) relationship between ivosidenib and 2-HG was analyzed in an m*IDH1* xenograft mouse model. Ivosidenib was well absorbed, showed low clearance, and moderate to long terminal half-life (5.3–18.5 hours) in rats, dogs, and monkeys. Brain to plasma exposure ratio was low (2.3%), plasma protein binding was high, and oxidative metabolism was the major elimination pathway. Ivosidenib had high cell permeability and was identified as a substrate for P-glycoprotein. There was moderate induction of cytochrome P450 (CYP) enzymes CYP3A4 and CYP2B6 but minimal CYP inhibition or autoinduction. Tumor 2-HG reduction appeared to be dose and drug-exposure dependent. Ivosidenib showed a favorable PK profile in several animal species, along with a clear PK/PD relationship demonstrating 2-HG inhibition, that translated well to patients with AML.

Significance Statement [80/80 words maximum]

Ivosidenib is a mutant IDH1 (mIDH1) inhibitor approved for the treatment of certain patients with m*IDH1* acute myeloid leukemia (AML). In Sprague-Dawley rats, beagle dogs, and cynomolgus monkeys, ivosidenib demonstrated a favorable pharmacokinetic profile, and in female BALB/c mice showed clear dose- and exposure-dependent inhibition of the oncometabolite, D-2-hydroxyglutarate, which is present at abnormal levels in m*IDH1* tumors. These findings led to the further development of ivosidenib and are consistent with data from patients with m*IDH1* cancers and healthy participants.

Introduction

Point mutations in isocitrate dehydrogenase (*IDH*) 1 and 2 are found in multiple tumors, including glioma, cholangiocarcinoma, chondrosarcoma, and acute myeloid leukemia (AML). Mutations in the metabolic enzymes IDH1 and IDH2 confer a gain-of-function neomorphic activity that results in conversion of α-ketoglutarate to the oncometabolite, D-2-hydroxyglutarate (2-HG) (Dang et al., 2009; Ward et al., 2010). This abnormal production of 2-HG can result in accumulation, with intracellular concentrations reaching 3–10 mM in samples from patients with mutant *IDH1* (m*IDH1*) AML (Yen et al., 2013). 2-HG competitively inhibits α-ketoglutarate–dependent dioxygenases, which participate in many cellular processes such as histone and DNA demethylation and adaption to hypoxia; their inhibition leads to alterations in the epigenetic state of cells and impaired cellular differentiation (Xu et al., 2011; Lu et al., 2012; Saha et al., 2014).

Ivosidenib (AG-120) is an inhibitor of the mIDH1 enzyme that is approved by the US Food and Drug Administration (FDA) for the treatment of adults with m*IDH1* relapsed or refractory AML and with m*IDH1* newly diagnosed AML who are ≥75 years old or who are ineligible for intensive induction chemotherapy (Agios Pharmaceuticals Inc., 2019). In preclinical studies, ivosidenib inhibited 2-HG in an m*IDH1* mouse xenograft tumor model, reduced intracellular 2-HG levels in m*IDH1*-expressing AML cells in vitro, and induced differentiation of primary patient AML m*IDH1* cells ex vivo (Popovici-Muller et al., 2018). US FDA approval was based on data from a phase I study evaluating the efficacy, safety, and pharmacokinetic (PK) profile of ivosidenib in patients with m*IDH1* advanced hematologic malignancies (ClinicalTrials.gov registration number NCT02074839) (DiNardo et al., 2018; Fan et al., 2020a). Clinical development of ivosidenib for the treatment of solid tumors with m*IDH1* is also ongoing, with a phase I study evaluating the safety, efficacy, and PK profile of ivosidenib in patients with advanced m*IDH1* solid tumors, including cholangiocarcinoma, chondrosarcoma, and glioma (ClinicalTrials.gov registration number NCT02073994) (Abou-Alfa et al., 2020; Fan et al., 2020b; Mellinghoff et al., 2020; Tap et al., 2020). In both these studies, the PK profile of ivosidenib was determined following both single and multiple dosing in dose-escalation and dose-expansion portions. During the escalation portions, ivosidenib doses of 100 mg b.i.d. and 300–1200 mg once daily (q.d.) were evaluated and, during the expansion portions, patients received the recommended dose of ivosidenib 500 mg q.d. Additional studies in healthy participants have evaluated the effect of food, ethnicity, and itraconazole on the PK of ivosidenib, and the absorption, metabolism, and excretion of radiolabeled ivosidenib (Dai et al., 2019; Prakash et al., 2019). Phase III randomized studies of ivosidenib in advanced m*IDH1* cholangiocarcinoma (ClarIDHy; ClinicalTrials.gov registration number NCT02989857) (Abou-Alfa et al., 2020) and in newly diagnosed m*IDH1* AML in combination with azacitidine (AGILE; ClinicalTrials.gov registration number NCT03173248) are ongoing.

Here, we report the preclinical in vitro and in vivo drug metabolism, PK, and pharmacodynamic (PD) profiles of ivosidenib in mouse, rat, dog, and monkey, the PK/PD relationship between ivosidenib and 2-HG inhibition in a mouse xenograft tumor model, and discuss the predictivity of these preclinical data for that observed in humans.

Materials and Methods

Ivosidenib (unlabeled, ^{14}C-, or deuterated ivosidenib [AGI-18070]) was synthesized by Agios Pharmaceuticals, Inc. for all in vitro and in vivo experiments. All work described was exploratory; it was conducted as a part of lead optimization that led to the selection of ivosidenib as a development candidate, and during further profiling of the molecule before clinical trials.

In Vitro Studies

Plasma Protein Binding

Protein binding was determined in human, monkey, dog, rat, and mouse plasma (mixed sex and pooled per species; supplied by Pharmaron Beijing Co., Ltd., Beijing, China) at ivosidenib concentrations of 0.2 μM, 1 μM, and 10 μM, using an ultracentrifugation method. All experiments were performed in duplicate. A 3 μl aliquot of working solutions [0.2, 1, and 10 mM in dimethyl sulfoxide (DMSO)] was mixed with 2997 μl of blank plasma at final concentrations of 0.2, 1, and 10 μM and then incubated at 37°C with 5% carbon dioxide for 30 minutes. After incubation, a 50 μl aliquot was collected from each plasma sample and treated as control samples. These control samples were mixed with 50 μl Dulbecco’s phosphate-buffered saline and 300 μl acetonitrile containing internal standards (200 nM imipramine, 200 nM labetalol, and 200 nM diclofenac) to precipitate proteins. Samples were vortexed for 2 minutes and centrifuged for 15 minutes at 20,000*g*. Supernatant was transferred to a new plate for liquid chromatography with tandem mass spectrometry (LC-MS/MS) analysis. The rest of the incubated samples were transferred into ultracentrifuge tubes and spun for 5.5 hours at 600,000*g* at 37°C. After ultracentrifugation, a 50 μl aliquot of supernatant was collected from the center of the ultracentrifuge tubes and mixed with 50 μl of blank plasma. The samples were then treated the same as noncentrifuged control samples. Ketoconazole samples were prepared in a similar manner and treated as the method control.

In vitro Metabolic Stability

The metabolic stability of ivosidenib was evaluated in liver microsomes (20-donor mixed-sex pool for humans, male Sprague-Dawley rat, male CD-1 mouse, male cynomolgus monkey, and male beagle dog; supplied by BD, Franklin Lakes, NJ). Ketanserin (control, 1 μM) and ivosidenib (1 µM) were incubated with human, monkey, dog, rat, and mouse liver microsomes (0.5 mg/ml in 0.1 M potassium phosphate buffer, pH 7.4) separately for 0, 5, 15, 30, and 45 minutes in 96-well plates. Reactions were initiated by addition of 15 µl of the reduced form of nicotinamide adenine dinucleotide phosphate (NADPH; final concentration at 2 mM) in 0.1 M potassium phosphate buffer (pH 7.4). At each time point, an aliquot of 135 µl acetonitrile containing Osalmid as the internal standard was added to the samples to stop the reaction. The plates were centrifuged to precipitate proteins and the supernatants were analyzed by LC-MS/MS for ivosidenib. In vitro intrinsic clearance (CL_{int}), scaled hepatic clearance (CL_{hep}), and hepatic extraction ratio (Eh) were calculated in microsomes from all species tested using the equations and species-specific scaling factors (Davies and Morris, 1993; Iwatsubo et al., 1997; Obach, 2000):

$$CL_{int}(\mu l/min/mg) = \frac{0.693}{t_{1/2}(min)} \cdot \frac{\mu l\ incubation}{mg\ of\ microsomal\ protein}$$

$$CL'_{int}(l/h/kg) = CL_{int} \cdot \frac{mg\ microsomal\ protein}{g\ of\ liver\ weight} \cdot \frac{g\ of\ liver\ weight}{kg\ of\ body\ weight} \cdot \frac{60\ min/h}{1000000\ \mu l/l}$$

$$CL_{hep}(l/h/kg) = \frac{Q_H \cdot CL'_{int}}{(Q_H + CL'_{int})}$$

$$Eh = \frac{CL_{hep}}{Q_H}$$

where $t_{1/2}$ is the half-life of % remaining vs time in the microsomal incubation and Q_H is the liver blood flow.

Metabolite Identification

For metabolite profiling and characterization, ivosidenib 100 µM was incubated in rat, dog, monkey, and human liver microsomes (1 mg protein/ml, pooled per species; supplied by BD Gentest™) in 1 ml of 100 mM phosphate buffer at 37°C for 120 minutes in the presence of 1 mM NADPH regeneration system. An additional 1 mM NADPH was added at 60 minutes after incubation. The reactions were stopped and extracted by adding 1 ml of ethyl acetate. Circulating metabolites were also assessed in rat and monkey plasma samples from ivosidenib non-good laboratory practice 7-day repeat-dose toxicology studies. Day 1 and Day 7 plasma samples from male Sprague-Dawley rats (250 mg/kg b.i.d. doses) and male cynomolgus monkeys (100 mg/kg b.i.d. doses) were pooled for metabolite identification. Pooled plasma samples were mixed with acetonitrile to precipitate proteins and the mixtures were centrifuged at 4000 rpm for 15 minutes at 4°C. Extractions (from liver microsomes) and supernatants (from plasma) were dried under nitrogen flow at room temperature and reconstituted in 75% methanol for LC-MS/MS analysis (with UV detection).

CYP Phenotyping

The role of human cytochrome P450 (CYP) enzymes in the metabolism of ivosidenib was evaluated with human liver microsomes and recombinant human CYP enzymes. [^{14}C]-ivosidenib (1, 10, and 100 µM) was first incubated for 120 minutes at 37ºC with pooled human liver microsomes (Xenotech Xtreme200, pool of 100 male and 100 female individuals, Catalog H2620; 0.5, 1, and 2 mg/mL protein), with and without an NADPH-generating system, to quantify the loss of [^{14}C]-ivosidenib as potential metabolites and assess the suitability of the analytical system. [^{14}C]-ivosidenib (10 and 100 µM) was then incubated with a panel of recombinant human CYP enzymes (1A2, 2B6, 2C8, 2C9, 2C19, 2D6, and 3A4; 25 pmol CYP per incubation) for 120 minutes at 37ºC. Ivosidenib metabolism was analyzed using an LC-MS/MS method with radiometric detection. To quantify substrate disappearance and metabolite formation, calibration standards were constructed with [^{14}C]-ivosidenib based on radiometric detection.

DMD Fast Forward. Published on July 28, 2021 as DOI: 10.1124/dmd.120.000234
This article has not been copyedited and formatted. The final version may differ from this version.

Drug-Drug Interaction Potential

CYP Inhibition

Human liver microsomes from nontransplantable donated livers from a mixed-sex pool of 16 individuals (supplied by XenoTech, LLC, Lenexa, KS) were prepared and characterized. To evaluate the potential of ivosidenib as an inhibitor of CYP enzymes, human liver microsomes were incubated with ivosidenib (at concentrations ranging from 0.05 to 50 µM) and marker substrates for CYP1A2 (phenacetin 40 µM), CYP2B6 (efavirenz 3 µM), CYP2C8 (amodiaquine 1.5 µM), CYP2C9 (diclofenac 6 µM), CYP2C19 (S-mephenytoin 40 µM), CYP2D6 (dextromethorphan 7.5 µM), and CYP3A4/5 (testosterone 70 µM, midazolam 4 µM). To distinguish between time-dependent and metabolism-dependent inhibition, ivosidenib was preincubated with human liver microsomes for 30 minutes without and with an NADPH-generating system, respectively, prior to the incubation with marker substrates. α-naphthoflavone for CYP1A2 (0.5 µM), orphenadrine for CYP2B6 (750 µM), monteleucast for CYP2C8 (0.05 µM), sulfaphenazole for CYP2C9 (2 µM), modafinil for CYP2C19 (250 µM), quinidine for CYP2D6 (0.5µM), and ketoconazole for CYP3A4/5 (0.15 µM for testosterone and 0.075 µM for midazolam marker substrates) were used as positive controls for direct inhibition. Furafylline for CYP1A2 (1 µM), phencyclidine for CYP2B6 (30 µM), gemfibrozil glucuronide for CYP2C8 (5 µM), tienilic acid for CYP2C9 (0.25 µM), S-fluoxetine for CYP2C19 (20 µM), paroxetine for CYP2D6 (0.3 µM), and troleandomycin for CYP3A4/5 (25 µM for testosterone and 7.5 µM for midazolam marker substrates) were used as positive controls for metabolism-dependent inhibition. Incubations were conducted at 37°C in 200 µl incubation mixtures (target pH 7.4) containing water, potassium phosphate buffer (50 mM), $MgCl_2$ (3 mM), EDTA (1 mM), an NADPH-generating system, and marker substrate. Marker substrate reactions were initiated by the addition of an aliquot of an NADPH-generating system and were automatically terminated at approximately 5 minutes by the addition of the appropriate internal standard and stop reagent, acetonitrile. The samples were centrifuged at 920*g* for 10 minutes at 10°C and the supernatant fractions were analyzed by LC-MS/MS.

When inhibition of a CYP enzyme was observed, the data were processed for the determination of IC_{50} values by nonlinear regression to the 4-parameter sigmoidal-logistic IC_{50} equation:

$$Y = Min + \frac{(Max - Min)}{(1 + (Conc/IC_{50})^{slope})}$$

where Min is set to zero and Max is set to 100 as percent of control values are utilized in the calculations.

CYP Induction

Three preparations of cryopreserved human hepatocytes (hereafter referred to as HC3-15, HC3-18, and HC5-25, all from male donors) supplied by XenoTech, LLC, were used to determine CYP induction and autoinduction potential of ivosidenib. Hepatocyte cultures were treated with ivosidenib or positive controls q.d. for three consecutive days. For evaluation of CYP induction, cells were cultured with supplemented modified Eagle's medium Dr Chee’s modification containing 0.1% v/v DMSO (vehicle, negative control), flumazenil (25 μM, negative control), one of seven concentrations of ivosidenib (0.1, 1, 5, 10, 25, 50, or 90 μM), or one of three known human CYP enzyme inducers, omeprazole for CYP1A2 (50 μM), phenobarbital for CYP2B6 (750 μM), or rifampin for CYP3A4/5 (10 μM). At 24 hours after the last treatment with ivosidenib and known CYP inducers, hepatocytes were incubated at 37°C for 30 minutes with marker substrates for CYP1A2 (phenacetin 100 μM), CYP2B6 (bupropion 500 μM), and CYP3A4/5 (midazolam 30 μM) in a total incubation volume of 200 μl.

Autoinduction

For evaluation of autoinduction, the same hepatocyte lots (HC3-15, HC3-18, and HC5-25) were incubated with modified Eagle's medium (Dr Chee's modification) containing 0.1% v/v DMSO (vehicle, negative control), one of four concentrations of ivosidenib (1, 10, 50, or 90 µM), or rifampin (10 µM) as a positive control for CYP3A4/5 induction with the same incubation conditions. At 24 hours after the last treatment of vehicle, ivosidenib, or rifampin, the autoinduction potential was assessed by measuring the intrinsic clearance of the CYP3A4/5 marker substrate midazolam (30 µM, incubated for 30 min) or the deuterated (d4) analog of ivosidenib (AGI-18070; 0.1 and 1 µM), incubated for up to 0.5, 1, 2, 4, 6, and 24 hours. Substrate reactions were started by the addition of the CYP probe substrate and stopped with acetonitrile. The samples were centrifuged at 2000*g* for 10 minutes at 2–8°C (CYP induction) or mixed thoroughly (autoinduction), and the supernatant fractions were analyzed by LC-MS/MS for the metabolites of probe substrates (acetaminophen for CYP1A2, hydroxybupropion for CYP2B6, and 1'-hydroxymidazolam for CYP3A4/5). Authentic metabolite standards and deuterated metabolites as internal standards were used in all assays. Following substrate incubations, hepatocytes from the same treatment groups were harvested with a lysis buffer (Buffer RLT, Qiagen, Germantown, MD) to isolate RNA, which was analyzed by quantitative reverse transcription polymerase chain reaction to assess the effect of ivosidenib on CYP1A2, CYP2B6, and CYP3A4 mRNA levels.

Fold changes in either activity or mRNA levels were determined by dividing the enzymatic rate or expression for each treatment group by that of the vehicle control. Fold increase was calculated as fold change – 1. The E_{max} and EC_{50} were calculated using a sigmoidal 3-parameter or sigmoidal Hill 3-parameter equation, where E_{max} was defined as the maximum fold induction observed in vitro and EC_{50} as the concentration of the inducer associated with half-maximal induction. Viability of hepatocytes and cytotoxic potential of ivosidenib in the hepatocyte incubations were assessed by two methods. The morphological integrity of hepatocytes after incubation was assessed using a Nikon TMS Microscope (Nikon Corporation) and a representative dish from each treatment group was photographed with an Accu-Scope 318 CU digital camera (Accu-Scope Inc). The potential of ivosidenib to cause cytotoxicity was also assessed based on the release of lactate dehydrogenase (LDH) into the culture medium (a measure of cell membrane integrity).

Experiments were performed in accordance with the current draft US FDA Guidance on Drug Interaction Studies (U.S. Department of Health and Human Services Food and Drug Administration, 2012) and current industry best practices (Bjornsson et al., 2003; Huang et al., 2008; Ogilvie et al., 2008).

Permeability

Cells were cultured on 24-well transwell plates for 21 days (Caco-2 cells) or 3–5 days [Madin-Darby Canine Kidney II (MDCKII) cells] prior to the experiment. Caco-2 cells were cultured in Eagle’s minimal essential medium supplemented with fetal bovine serum (8.9%), nonessential amino acids (0.1 mM), and penicillin-streptomycin (45 U/ml and 45 µg/ml, respectively) in a humidified culture chamber (37 ± 1°C, 95% ± 5% relative humidity, and 5% ± 1% CO_2). MDCKII P-glycoprotein (P-gp), MDCKII breast cancer resistance protein (BCRP), and control MDCKII cells were cultured in Dulbecco's modified Eagle's medium supplemented with fetal bovine serum (10%) and penicillin-streptomycin (45 U/ml and 45 µg/ml, respectively) in a humidified culture chamber (37 ± 2°C, 95% ± 5% relative humidity, and 5% ± 1% CO_2).

Permeability incubations were carried out in incubation media (Hank's Balanced Salt Solution supplemented with 25 mM HEPES and 25 mM glucose) at 37 ± 2°C. Culture media was removed, and incubation media was added to the cells. The transepithelial resistance value was recorded approximately 10 minutes after the incubation media was added, and the cells were warmed to 37 ± 2°C for 30–60 minutes.

To determine whether ivosidenib is a substrate for P-gp or BCRP, bidirectional permeability of [^{14}C]-ivosidenib was measured in two test systems: across a Caco-2 cell transwell system using two concentrations of [^{14}C]-ivosidenib (5 and 20 μM), and across MDCKII cells overexpressing P-gp or BCRP with [^{14}C]-ivosidenib 5 μM in the presence and absence of P-gp inhibitors (valspodar or verapamil) or a BCRP inhibitor (Ko143). The ability of ivosidenib to inhibit the human efflux transporters, human P-gp and BCRP, was evaluated in vitro by measuring the bidirectional permeability of a probe substrate (digoxin for P-gp and prazosin for BCRP) across a monolayer of Caco-2 or MDCKII overexpressing BCRP (MDCKII-BCRP) cells, respectively, in the presence of ivosidenib (5 and 100 μM).

In the evaluation of ivosidenib as a P-gp/BCRP inhibitor, incubation media with probe substrate (digoxin 10 μM or prazosin 1 μM) containing the solvent control, control inhibitor (valspodar [10 μM] or verapamil [60 μM] for P-gp, and Ko143 [1 μM] for BCRP), or test article was added to the donor chamber. Incubation media containing the solvent control, control inhibitor, or test article was added to the receiver chamber. Samples (100 μl) were collected from the receiver compartment at 120 minutes.

In the evaluation of ivosidenib as a P-gp/BCRP substrate in a Caco-2 cell transwell system, incubation media with the test article (5 and 20 μM) was added to the donor chamber and incubation media was added to the receiver chamber. The positive control, digoxin (10 μM), in incubation media containing the solvent control or control inhibitor was added to the donor chamber, and incubation media containing the solvent control or control inhibitor was added to the receiver chamber. Samples (100 µl) were collected from the receiver compartment at 15, 30, and 120 minutes. For all drug transporter experiments in wells in which the recovery was calculated, samples (20 µl) were taken from the donor chambers at the start of the incubation (time zero) and after the final time point (120 minutes). Samples containing digoxin or prazosin were mixed with internal standard and analyzed by LC-MS/MS.

In Vivo Studies

In Vivo *PK Profiling in Rat, Dog, and Monkey*

All the studies were conducted according to approved institutional animal care and use protocols. All animals were housed in individual stainless-steel cages with wire mesh floors and plastic netting, which allowed separate collection of urine from feces. The room environment was well controlled, ventilating at least 15 times/h with lighting 12 h/day, and an approximate temperature of 20–24°C (rats) or 20–29°C (dogs, monkeys) and approximate humidity of 40%–70% (rats) or 30%–70% (dogs, monkeys). Water was freely available for all animals. Ivosidenib was formulated as a solution in 5% solutol HS for i.v. dosing and as a suspension in 0.5% methylcellulose and 0.2% Tween 80 for p.o. dosing in all three species. Single-dose ivosidenib was administered intravenously (i.v.; i.v. bolus to rats and 10-minute i.v. infusion to dogs and monkeys) at 1 mg/kg [via the foot dorsal vein (rats) or cephalic vein (dogs, monkeys)] or by oral gavage (p.o.) at 10 mg/kg. Animals in the p.o. groups were fasted overnight and fed 4 hours postdose; the i.v. groups were not fasted. For i.v. dosing, formulation concentrations were 0.5 mg/ml for rat and 1 mg/ml for dog and monkey. For p.o. dosing, formulation concentrations were 2 mg/ml for rat and 5 mg/ml in dog and monkey.

Male Sprague-Dawley rats were approximately 6–8 weeks old and 200–300 g in weight at the onset of treatment. Male beagle dogs were at least 5 months old and approximately 8–10 kg in weight. Male cynomolgus monkeys were at least 3 years old and approximately 3–4 kg in weight at the onset of treatment.

Blood samples were collected from rats (both i.v. and p.o. groups) at predose and 5, 15, and 30 minutes and 1, 2, 4, 8, and 24 hours postdose. In dogs and monkeys, blood samples were collected at predose and 5, 10, 15, and 30 minutes and 1, 2, 4, 8, and 24 hours postdose in the i.v. group, and at predose and 5, 15, and 30 minutes and 1, 2, 4, 8, and 24 hours postdose in the p.o. group. All blood samples were collected into test tubes containing K_2EDTA; blood samples were centrifuged to obtain plasma. Urine was collected from all animals in the i.v. groups at 0–4 hour, 4–8 hour, and 8–24 hour time intervals and stored at –70°C until analysis. The ivosidenib concentration in plasma and urine was quantified using LC-MS/MS. The lower limit of quantification was 3.00 ng/ml at a plasma sample volume of 15 µl in rats, and 1.00 ng/ml at a plasma sample volume of 30 µl in dogs and monkeys.

Plasma PK parameters calculated include CL, volume of distribution at a steady state (V_{ss}), half-life ($t_{½}$), maximum observed plasma concentration (C_{max}), time to maximum concentration (T_{max}), area under the concentration-time curve (AUC) from time 0 to 12 hours postdose ($AUC_{0–12h}$), AUC from time 0 to 24 hours postdose ($AUC_{0–24h}$), AUC extrapolated to infinity ($AUC_{0–inf}$), and oral bioavailability (F). All PK parameters were calculated using total concentrations (without applying plasma protein binding correction). PK analysis of plasma concentration data was performed using WinNonlin® (Version 6.2, Pharsight Corp., Mountain View, CA). PK parameters were estimated using a noncompartmental model method and AUC was calculated using the linear trapezoidal rule.

Distribution in Plasma, CSF, and Brain in Rat

Distribution of ivosidenib was evaluated in plasma, cerebrospinal fluid (CSF), and brain of male Sprague-Dawley rats aged approximately 6–8 weeks old and 240–270 g in weight at the onset of treatment. Rats received a single 50 mg/kg ivosidenib p.o. Blood, brain tissue, and CSF samples were collected at 1, 4, 8, and 24 hours postdose. Animals were euthanized with pure carbon dioxide inhalation. The CSF was collected by direct puncture with a butterfly needle into the cisterna magna. A piece of white paper was used to monitor color change in the sample during collection, with the clear sample drawn into the syringe. The whole brain was collected, rinsed with cold saline, dried on filtrate paper, weighed, and snap frozen by placing into dry ice. The concentration of ivosidenib in plasma, brain homogenates, and CSF samples was determined using an LC-MS/MS–based method. The lower limit of quantification was 3.00 ng/ml at a plasma sample volume of 15 µl.

Excretion of Unchanged Parent Compound

Excretion in Urine (Rat, Dog, and Monkey)

Excretion of unchanged parent compound in urine was evaluated as part of the aforementioned in vivo PK profiling of ivosidenib in rats, dogs, and monkeys. Animals received a single i.v. dose (1 mg/kg) of ivosidenib and the amount of unchanged ivosidenib recovered from urine during the 24-hour sampling period was determined by LC-MS/MS.

Excretion in Bile (Rat)

Biliary excretion of unchanged parent compound was evaluated in male Sprague-Dawley rats aged approximately 6–8 weeks old and 250–300 g in weight at the onset of treatment. Housing and care conditions were the same as described for in vivo PK profiling.

Rats were anesthetized with 1.5 ml/kg ketamine cocktail and the bile duct was then cannulated for bile collection. After allowing recovery from surgery and anesthesia for at least 24 hours, these bile-duct cannulated rats received a single i.v. dose of ivosidenib 1 mg/kg via the dorsal foot vein. Bile samples were collected predose and 0–2 hours, 2–4 hours, 4–8 hours, and 8–24 hours after i.v. administration. A 15 µl aliquot of bile sample was mixed with 100 µl acetonitrile containing internal standard (diclofenac 20 ng/ml) for protein precipitation. The mixture was vortexed at 1500 rpm for 2 minutes and centrifuged at 14,000 rpm for 5 minutes, and supernatant analyzed by LC-MS/MS. Using a bile sample volume of 15 µl, linearity was achieved in the ivosidenib concentration range of 1–3000 ng/ml.

Xenograft Mouse Model: PK/PD Relationship Between Ivosidenib and 2-HG Reduction

For studies investigating the PK/PD relationship between ivosidenib exposure and inhibition of 2-HG production after multiple oral doses, an HT1080 xenograft mouse model (R132C mutation in IDH1) was used. Briefly, female BALB/c nude mice were inoculated subcutaneously on the flank with 3.0×10^6 HT1080 cells. On day 14 after inoculation, the mice were randomized based on tumor volume when tumor size reached approximately 100–900 mm^3. The mice were then dosed orally with multiple doses of vehicle or ivosidenib; oral doses were prepared as a homogeneous suspension in 0.5% methylcellulose and 0.2% Tween 80 in water.

Animals were dosed orally with three repeat doses of vehicle (n = 12 per dose group) or three repeat doses of ivosidenib 20, 50, or 150 mg/kg (n = 20 per dose group) every 12 hours. In the vehicle groups, blood and tumor tissue samples were collected from mice at 1, 12, and 24 hours after the last dose (n = 4 per time point). In the active-dose groups, blood samples were collected from mice at 1, 3, 8, 12, and 24 hours after the last dose (n = 4 per time point).

The PK/PD relationship between ivosidenib exposure ($AUC_{0–12h}$) and the average 2-HG concentration over a 12-hour period was established by an inhibitory E_{max} model:

$$E = E_0 \cdot \left[1 - \left(\frac{AUC}{AUC + EAUC_{50}}\right)\right]$$

Where E is average 2-HG tumor concentration after ivosidenib dosing, E_0 is the baseline 2-HG concentration (in the vehicle group), AUC is the ivosidenib plasma $AUC_{0–12h}$, and $EAUC_{50}$ is the ivosidenib plasma $AUC_{0–12h}$ causing 50% of maximal effect. $EAUC_{90}$ (ivosidenib AUC resulting in 90% 2-HG reduction) and $EAUC_{97}$ (ivosidenib AUC resulting in 97% 2-HG reduction) were then derived from $EAUC_{50}$ parameter.

Human PK and Dose Projection

Projection of human CL was performed using standard allometric principles. In vitro and/or vivo CL parameters in rat, dog, monkey, and human were considered for human CL projection. Allometric scaling of total clearance and unbound clearance was performed using the equation:

$$CL_{human} = a \,. W^b$$

where a is the coefficient, b is the exponent, and W is the body weight. Human V_{ss} was projected to be (a) the average of the estimates in the animal species, (b) based on allometric scaling of total V_{ss}, (c) based on allometric scaling of unbound V_{ss}, and (d) by Oie-Tozer method (Oie and Tozer, 1979; Obach et al., 1997). Fraction unbound in tissues (f_{ut}) for each pre-clinical species was calculated by the equation:

$$f_{ut} = \frac{V_r \cdot f_u}{\left[V_{ss} - V_p - (f_u \cdot V_e)\right] - \left[(1 - f_u) \cdot \frac{R_e}{i} \cdot V_p\right]}$$

Human V_{ss} was calculated using the equation:

$$V_{ss(human)} = V_p + \left[f_{u(human)} \cdot V_e\right] + \left\{\left[1 - f_{u(human)}\right] \cdot \frac{R_e}{i} \cdot V_p\right\} + V_r \cdot \frac{f_{u(human)}}{f_{ut(average)}}$$

where V_r is the volume into which the drug distributes minus the extracellular space, V_p is the plasma volume, f_u is the fraction unbound, V_e is the extracellular volume minus the plasma volume, $R_{e/i}$ is the ratio of the total amount of protein in extracellular fluids outside the plasma to that in the plasma (the values for these physiological parameters were from the literature (Obach et al., 1997)).

Oral bioavailability of ivosidenib was projected based on the observed bioavailability in the animal species. Exposures in the mouse PK/PD model associated with 97% 2-HG reductions were targeted to arrive at human dose projections. Efficacious human dose was predicted based on the projected human CL, oral bioavailability, and the targeted exposures based on the PK/PD model.

Bioanalytical Methods

Bioanalytical methods for the in vivo and in vitro studies are detailed in the Supplemental Data.

Results

Pharmacokinetics in Preclinical Species

Following single-dose i.v. administration of 1 mg/kg, ivosidenib demonstrated low plasma total CL (0.2 l/h/kg) in rats and monkeys and very low CL (0.02 l/h/kg) in dogs. Volume of distribution at steady state (V_{ss}) was 2.1 l/kg, 1.24 l/kg, and 0.73 l/kg in rat, monkey, and dog, respectively. Terminal half-life ($t_{1/2}$) was 8.9 hours, 5.3 hours, and 18.5 hours in rat, monkey, and dog, respectively (Fig. 1; Table 1). Following single-dose oral administration of 10 mg/kg as a suspension, ivosidenib was well absorbed in rats, dogs, and monkeys, appearing in the blood stream 15 minutes after dosing, with a T_{max} of 2.7, 9.5, and 5.3 hours, respectively, and acceptable/good oral F of 39.5%, 25.9%, and 53.8% in dogs, rats, and monkeys, respectively (Fig. 1; Table 1).

Distribution in Plasma, CSF, and Brain in Rat

Following a single oral dose of ivosidenib 50 mg/kg in male rats, the plasma, CSF, and brain total exposures ($AUC_{0–24h}$) were 65093, 350, and 1481 h•ng/ml, respectively, and T_{max} was 4 hours in all three tissues. Distribution of ivosidenib was low in the brain (brain to plasma ratio = 2.28%) and CSF (CSF to plasma ratio = 0.538%), suggesting low brain penetration.

Plasma Protein Binding

Evaluation of 0.2 μM, 1.0 μM, and 10 μM of ivosidenib in human, monkey, dog, rat, and mouse plasma showed that the plasma protein binding (PPB) of ivosidenib was high (82%–98%), though it differed across species and concentrations (Table S1). Across species, plasma protein binding was 1%–9% lower at the 10 μM concentration of ivosidenib compared with 0.2 μM and 1 μM.

In vitro Metabolic Stability

In vitro metabolic stability of ivosidenib was demonstrated in mouse, rat, dog, monkey, and human liver microsomes. Ivosidenib showed low CL_{int} uncorrected for protein or microsomal binding of ivosidenib in liver microsomes derived from mice (3.2 µl/min/kg), rats (10.4 µl/min/kg), monkeys (3.1 µl/min/kg), and humans (4.9 µl/min/kg). Corresponding CL_{hep} and Eh were low in mice (0.66 l/h/kg and 0.12), rats (0.84 l/h/kg and 0.25), monkeys (0.24 l/h/kg and 0.09), and humans (0.28 l/h/kg 0.16). Ivosidenib did not show any measurable clearance in dog liver microsomes. The Eh in liver microsomes across species ranged from a low of 0.09 in monkeys to a high of 0.25 in rats, bracketing the value in human liver microsomes of 0.23 (Table S2).

Excretion

After i.v. single-dose administration, the amount of unchanged ivosidenib recovered from the urine in 24 hours was negligible in rats (1.6% of dose), dogs (0.94%), and monkeys (0.53%). Urinary excretion of parent compound, expressed as renal clearance (CL_r), is summarized in Table 1. In addition, amount of unchanged ivosidenib recovered in bile of bile-duct cannulated rats was negligible (0.26% of IV dose).

Metabolite Identification

Four mono-oxygenated metabolites of ivosidenib [M1 – M4; $(M + H)^+ = 599$], determined by in vitro metabolite identification, were formed at various concentrations in rat, dog, monkey, and human liver microsomes (tentative structures based on fragmentation patterns are represented in Fig. 2). Ivosidenib, with a molecular weight of 583 g/mol had a retention time (RT) of 16.8 minutes. M1 (RT 14.9 minutes) was formed at a relatively higher concentration in liver microsomes from all four species than M2 (RT 15.7 minutes), M3 (RT 15.9 minutes), or M4 (RT 16.2 minutes). Only M1 was detectable using a UV detector (280 nm); M2-M4 were undetectable using UV detector and were identified based on MS/MS analysis. No humanspecific metabolites were observed. Characteristic fragmentation ions of the parent include m/z 476, 370, 214, and 186. The shifts from these fragment ions of the parent were used to assign the modification sites of metabolites. M1 showed the characteristic fragment ions of m/z 492 (476+16), 386 and 186, indicating the right side of the molecule remains intact and the hydroxylation occurred in the middle part of the molecule. M2 showed the characteristic fragment ions of m/z 492 (476+16), 370, and 202 (186+16), indicating the right side of the molecule modified by hydroxylation. M3 showed same characteristic fragment ions as M2, m/z 492 (476+16), 370 and 202 (186+16), indicating the right side of the molecule modified by hydroxylation. M4 showed the characteristic fragment ions of m/z 476, 370, 214 and 186, indicating the left side of the molecule modified by hydroxylation.

Assessment of plasma samples from 7 days of ivosidenib dosing in rats and monkeys identified that ivosidenib (RT 15.1 minutes) undergoes oxidative metabolism to form two major monohydroxylated metabolites in vivo: M1 (RT 13.3–13.4 minutes) and M2 (RT 14.3–14.4 minutes), both $[M + H]^+$ = 599. There were no qualitative differences between the profiles obtained from day 0 versus day 6 samples in either species. Profiles for these metabolites were similar to those of the M1 and M2 metabolites observed in vitro, but metabolites corresponding to M3 and M4 were not observed in the plasma of either species. Two additional metabolites, M5 (RT 13.9 minutes, $[M + H]^+$ = 601) and M6 (RT 15.4 minutes, $[M + H]^+$ = 616), which are consistent with the amide and the methyl ester derivatives due to the metabolism of the cyanide group, were identified in the monkey plasma but were not detected in rat plasma or rat or monkey liver microsomes (Fig. 2). M5 showed the characteristic fragment ions of m/z 494 (476+18) and 204 (186+18), indicating the right side of the molecule was modified by addition of 18, which is consistent with cyanide hydrolysis to amide. M6 showed the characteristic molecular ion m/z 618 (583-N+46) and fragment ions of m/z 509 (476-N+46) and 219 (186-N+46), indicating the change of nitrogen rule and the structure is consistent with a methyl ester to replace the cyanide group. Except for this finding, in vitro and in vivo metabolic profiles were similar in both rats and monkeys. No phase II metabolites were observed in the plasma of either species.

CYP Phenotyping

In both human liver microsomes and recombinant human CYP enzymes, the extent of metabolism of [^{14}C]-ivosidenib to potential metabolites was minor under the experimental conditions. The disappearance of [^{14}C]-ivosidenib over the 120-minute incubation period in the human liver microsomes with NADPH was less than 15% at 1, 10, and 100 µM. Four radioactive peaks (C3, C4, C5a, and C5b) were identified as monooxygenated metabolites (+16 amu mass shift from the parent compound). The radioactive peak C2 was identified as cyclobutyl N-dealkylation metabolite (m/z 495). These radioactive components were quantified based on a calibration curve constructed with the parent compound. The percent conversion of parent compound to C3 and C5 was <3% and was not quantifiable for C2 and C4 over the incubation period. Due to this low turnover, a rate of metabolism could not be determined with any degree of certainty.

After incubation of 10 and 100 µM [^{14}C]-ivosidenib, less than 4% loss of parent compound was observed with the exception of rCYP3A4, which resulted in 17% loss. All of the radiometric metabolites observed in the human liver microsomes were also observed in all recombinant enzyme incubations. Based on the formation of metabolite peaks, several CYP enzymes (2B6, 2C8, 2D6, and 3A4; 3A4 being the predominant) appeared to contribute to the metabolism of [^{14}C]-ivosidenib. None of these metabolites could be observed with CYP1A2, CYP2C9, or CYP2C19. Due to the low conversion of [^{14}C]-ivosidenib to metabolites by NADPHfortified human liver microsomes, a chemical inhibition experiment was not performed to further ascertain the role of individual CYP isoforms.

Drug-Drug Interaction Potential

CYP Inhibition

In human liver microsomes, there was evidence of weak direct inhibition of CYP2C8, CYP2C19, CYP2D6, and CYP3A4/5 (testosterone 6β-hydroxylation and midazolam 1'-hydroxylation) of 44%, 31%, 44%, 33%, and 48% inhibition, respectively, at the highest concentration of ivosidenib evaluated (50 μM). IC_{50} values were thus >50 μM (Table 2). There was little or no evidence of direct inhibition of CYP1A2, CYP2B6, or CYP2C9 by ivosidenib and IC_{50} values were >50 μM. In addition, there was little or no evidence of time- or metabolism-dependent inhibition by ivosidenib for any of the CYP enzymes evaluated, as determined by an IC_{50} shift experiment, suggesting that formation of reactive metabolites is unlikely.

CYP Induction

CYP induction studies were conducted in hepatocyte cultures from 3 donors: HC3-15, HC3-18, and HC5 25. The results were variable for cells from different human donors with ivosidenib treatment. Ivosidenib showed little to no effect on CYP1A2 activity or CYP1A2 mRNA levels (< 2 fold), with the exception of a 5.55-fold change in CYP1A2 activity in HC3-15 and a 3.74- and 2.48-fold change in CYP1A2 mRNA levels in HC3-15 and HC3-18 upon treatment with 90 μM ivosidenib (Fig. S1). Treatment with positive control (omeprazole 50 μM) increased CYP1A2 activity up to 35.4-fold and mRNA levels up to 200-fold.

Treatment with ivosidenib caused an increase in CYP2B6 activity with up to a 9.02-fold change at 25 μM ivosidenib in HC3-15 and up to a 4.37-fold change at 5 μM ivosidenib in HC3-18 (Fig. S1). In both cultures, the increase in CYP2B6 activity was followed by a slight decrease in CYP2B6 activity at higher concentrations of ivosidenib. There was <2-fold induction at any concentration in HC5-25. The positive control phenobarbital induced 33.6, 26.6, and 6-fold induction in the three cultures (21.6 ± 15.2) (Fig. S1).

Treatment with up to 90 μM ivosidenib caused an increase in CYP2B6 mRNA levels in all 3 hepatocyte cultures, with up to a 5.57- fold (HC3-15) and 3.93-fold (HC3-18) change at 90 μM ivosidenib and up to a 2.55-fold change at 10 μM ivosidenib in HC5-25 followed by a slight decrease in CYP2B6 mRNA levels at higher concentrations (Fig. S1). The positive control phenobarbital induced a 13.0 ± 4.7- fold response.

Treatment with ivosidenib caused an increase in CYP3A4/5 activity, with up to a 4.86-fold change at 10 μM ivosidenib in HC3-15 and up to a 3.58-fold change at 5 μM in HC5-25 (Fig. S1). In both cultures, the increase in CYP3A4/5 activity was followed by a decrease in CYP3A4/5 activity at higher concentrations of ivosidenib. The positive control rifampin induced a 6.99 ± 3.55-fold change in activity. Treatment with up to 90 μM ivosidenib caused an increase in CYP3A4 mRNA levels in all 3 hepatocyte cultures, with up to a 219 fold change at 90 μM in HC3-15 and up to a 25.1- (HC3-18) and 6.50- (HC5-25) fold change at 50 μM ivosidenib, followed by a slight decrease in CYP3A4 mRNA levels at the highest concentration (90 μM). The positive control rifampin induced a 131, 34.2, and 9.62-fold change in mRNA levels in the three cultures.

E_{max} and EC_{50} values for fold-change in CYP activity and fold-change in mRNA are presented in Table 3. Activity E_{max} was higher than mRNA E_{max} for CYP1A2 in HC3-15, and for CYP2B6 in HC3-15 and HC3-18 (Fig. S2-S4).

Treatment of cultured hepatocytes with up to 50 µM ivosidenib for three consecutive days did not cause any detectable cytotoxicity based on cell morphology. Treatment with 90 µM ivosidenib exhibited morphological changes in one of the three hepatocyte cultures (HC5-25) in the induction study and two out of the three cultures (HC3-18 and HC5-25) in the autoinduction study. The cells were intact, but had cell elongation or shriveling, swollen nuclei, and grainy cytoplasm with increased vacuoles visible.

Autoinduction

In vitro assessment in cryopreserved human hepatocyte cultures (from three donors) indicated that ivosidenib is not able to induce its own metabolism. Following treatment with the CYP3A4 inducer, rifampin, or ivosidenib at concentrations of up to 90 µM for three consecutive days, there was no evidence for autoinduction as measured by clearance of the deuterated analog of ivosidenib at both 0.1 and 1.0 µM (Table 4). Furthermore, induction by rifampin did not significantly change the CL_{int} of ivosidenib, whereas rifampin increased the CL_{int} of midazolam by 6.5 ± 1.7-fold using the same system.

There was no significant increase in LDH release following treatment with up to 90 µM ivosidenib, indicating intact cell membranes, and hence the absence of cytotoxicity.

Permeability and Transporter-Based Drug-Drug Interaction Potential

Ivosidenib showed high apparent permeability (13.1 and 19.2 × 10^{-6} cm/s at 5 and 20 µM, respectively) in the Caco-2 cell transwell system. Efflux ratios for [^{14}C]-ivosidenib 5 µM and 20 µM were 4.28 and 2.33, respectively, indicating that ivosidenib could be a substrate for efflux pumps. In experiments conducted to measure the permeability of [^{14}C]-ivosidenib 5 µM across

DMD Fast Forward. Published on July 28, 2021 as DOI: 10.1124/dmd.120.000234
This article has not been copyedited and formatted. The final version may differ from this version.

MDCKII-P-gp and MDCKII-BCRP cells, the net efflux ratios in the absence of inhibitors were 12.4 and 0.590, respectively. In the presence of P-gp inhibitors verapamil or valspodar, the net efflux ratio was reduced to 1.75 and 1.72, respectively (approximately 7-fold) in MDCKII-P-gp cells. In MDCKII-BCRP cells, the presence of a BCRP inhibitor Ko143 had little impact on the net efflux ratio (0.859). These findings indicate ivosidenib is a substrate of P-gp but not BCRP (Tables 5 and 6).

Ivosidenib at 5 μM and 100 μM inhibited the transport of the P-gp substrate digoxin across Caco-2 cells by 48% and 99%, respectively; transport of the BCRP substrate prazosin across MDCKII-BCRP cells was inhibited by 17% and 48%, respectively. These data indicate that ivosidenib is an inhibitor of P-gp and a weak inhibitor of BCRP.

PK/PD Relationship Between Ivosidenib and 2-HG Reduction

In the mouse HT1080 xenograft tumor model, inhibition of tumor 2-HG production appeared to be dose and drug-exposure dependent [Fig. 3; single dose data previously published (Popovici-Muller et al., 2018)]. Tumor 2-HG reduction to baseline levels of wild-type tissue was achieved following three consecutive doses of ivosidenib of ≥20 mg/kg b.i.d. (Table 7). The PK/PD relationship between ivosidenib exposure and average concentration of 2-HG in that 12-hour period was explained by an inhibitory E_{max} model. The estimated efficacious $AUC_{0–12h}$ that resulted in sustained 50%, 90%, 97% tumor 2-HG reduction were 398, 3600 and 12,900 h•ng/ml, respectively (Fig. 4 and Table 8). The exposure that led to 97% 2-HG reduction was used to project the efficacious dose in humans. At these doses, 2-HG reduction was sustained for up to a 12 hour dosing interval, although the study was done with only three b.i.d. doses. In vitro IC_{50} in HT1080 cells with an IDH1-R132C mutation was 8 ± 4 nM (Popovici-Muller et al., 2018), and in vivo free IC_{50} in the present study, calculated based on average exposure corrected for average PPB, was 6.2 nM. In vivo total IC_{97}, calculated from $EAUC_{97}$ was 1075 ng/mL.

Prediction of Human PK and Efficacious Dose

Human total CL was predicted using standard allometric scaling principles. In vivo CL in dogs was approximately 10-times lower than in rats and monkeys and no liver microsomal CL was observed in dogs. Simple allometry using rat, dog, and monkey CL resulted in a poor correlation (R^2=0.60) and a low exponent (0.554), with a projected human CL of 0.02 l/h/kg. Allometric scaling of unbound CL improved the correlation (R^2=0.989) and the projected CL was 0.056 l/h/kg. In vitro Eh correction could not be applied as measurable liver microsomal clearance was not seen in dogs.

As the main aim of the human PK projection was to assess the developability of ivosidenib in humans, and to recommend the dose and dosing frequency, PK data from dogs were excluded from allometric scaling to arrive at a worst-case scenario of human CL, and the simple allometry using rat and monkey projected the human CL of 0.2 l/h/kg, consistent with the human in vitro hepatic CL of 0.28 l/h/kg.

Projected human V_{ss} estimates were 1.67 l/kg (species average), 0.49 l/kg (allometry of total V_{ss}), 1.30 l/kg (allometry of unbound V_{ss}), and 0.76 l/kg (Oie-Tozer method). Based on the observed bioavailability with the free form of ivosidenib in suspension formulation, and additional formulation work with the prototypical tablet formulation in monkey (data not included), the oral bioavailability of ivosidenib in humans was projected to be between 37% and 52.9%. Based on these data, the efficacious oral dose of ivosidenib in humans is projected to be in the range of 760–1080 mg/dose b.i.d. The estimated C_{max} at human efficacious dose levels is approximately 1510 ng/ml (or 2.59 μM).

Discussion

The current manuscript embodies the in vitro and in vivo PK and metabolism properties of ivosidenib that were generated during the developability assessment before entering clinical trials. The PK profile of ivosidenib in rat, dog, and monkey was characterized by low CL, moderate V_{ss}, acceptable oral bioavailability, and $t_{1/2}$ of 5.3 to 18.5 hours. There was a general agreement between in vitro and in vivo CL in that ivosidenib showed low CL, although there were numerical differences. The PPB of ivosidenib was high and differed across species, with dogs showing distinctly higher binding.

These cross-species differences introduced uncertainty in the human PK and dose projections. Projected human V_{ss} showed a range (0.49–1.36 l/kg) based on the four methods used. For CL, allometric scaling of unbound CL projected a lower human CL. However, to avoid the risk of not covering the scenario of b.i.d. dosing in the clinic, a conservative projection scenario of higher CL (0.2 instead of 0.056 l/h/kg) was used. The mean CL/F after single 500 mg oral doses in the clinical trials were 0.09 l/h/kg (Prakash et al., 2019) and 0.04 to 0.07 l/h/kg (Dai et al., 2019) in healthy participants, and 0.05 l/h/kg in patients with advanced m*IDH1* hematologic malignancies (Fan et al., 2020a). Ivosidenib showed good exposure and long-half-life in patients with advanced solid tumors (Fan et al., 2020a). As ivosidenib has not been dosed by the i.v. route in humans, CL can be inferred to be ≤ CL/F. Retrospective comparison suggests that the PPB-corrected CL estimate (0.056 l/h/kg) could have been used for the human PK and dose projections. However, the conservative assumption did not impact its clinical development path. Although conservatively predicted to be a b.i.d. drug, ivosidenib demonstrated PK properties in human patients that were conducive to a q.d. regimen.

In this study, brain penetration of ivosidenib was low in rat after a single dose, with a brain to plasma total exposure ratio of 2.3% and a CSF to plasma ratio of 0.54%, consistent with findings in an orthotopic glioma mouse model (3.5–3.9% after multiple doses) (Nicolay et al., 2017). Despite low brain penetrance, brain exposure of ivosidenib was sufficient to reduce 2-HG levels by up to 85% in brain tumors (Nicolay et al., 2017). Brain penetrance of ivosidenib was higher (brain to plasma total concentration ratios of 13% [250 mg q.d.] and 10% [500 mg q.d.]) in a phase I, open-label, perioperative study in patients with recurrent, m*IDH1*, low-grade glioma, with suppression of 2-HG (91.1%) seen in resected m*IDH1* gliomas (Mellinghoff et al., 2019). These findings demonstrate the utility of measuring the target engagement biomarker in the target tissue (glioma tumors in this case) in addition to measuring brain to plasma drug ratios.

Unbound fraction (f_u) of ivosidenib in human plasma was slightly higher at 10 µM (8.4%) compared with 0.2 µM (4.2%) and 1 µM (4.6%). In a study assessing the effect of hepatic impairment on the PK of ivosidenib, ex vivo mean unbound fractions at C_{max} (~5 µM at 3 hours post dose) in two cohorts of healthy human participants with normal hepatic function were 2.48% and 1.75%, and f_u decreased at lower concentrations (later sampling time points of 48 hours and 168 hours) (Fan et al., 2021). Binding affinities of ivosidenib to albumin and alpha-1 acid glycoprotein have not been determined.

Unchanged ivosidenib recovered in urine of rats, dogs, and monkeys was negligible. Biliary clearance of unchanged ivosidenib in rats was also negligible. Together, these results suggest that the majority of ivosidenib in these species is cleared by metabolism. Acceptable in vitro to in vivo correlation for CL indicated that any additional clearance pathways would be minor. While the CL/F in healthy human participants was low (0.09 l/h/kg) (Prakash et al., 2019), and agreed in general with the low CL projection, urinary excretion of unchanged parent compound after a 500 mg single p.o. dose was 9.9%, and higher than the excretion in rat, dog, and monkey (<2%). Different sampling durations in the animal species (24 hours) and humans (360 hours) could be a factor for this difference in urinary excretion estimates. A fecal recovery of 67.4% of oral dose as unchanged drug is indicative of unabsorbed drug, and biliary and intestinal excretion. As the absolute oral bioavailability is not known in humans, extrapolation of the relative contribution of metabolism to the overall clearance from non-clinical studies to the clinical study is likely inaccurate.

The routes of metabolism for ivosidenib appeared to be via multiple CYP enzymes, with CYP2B6, CYP2C8, CYP2D6, and CYP3A4 all contributing to the metabolism of ivosidenib. While CYP3A4 appeared to be a major enzyme, the relative contribution of each enzyme could not be accurately determined due to the low turnover of ivosidenib. The minor role of CYP2D6 is reflected by the observation that CYP2D6 genotype had no effect on ivosidenib exposure (Prakash et al., 2019). Mono-oxygenated metabolites (M1–M4) were the major metabolites in the cross-species in vitro liver microsome incubations. Two of these metabolites (M1 and M2) and two additional metabolites (amide and methyl ester derivatives of ivosidenib; M5, M6) were present in monkey plasma. After a single 500 mg dose of [^{14}C]-ivosidenib in healthy participants, a total of 13 metabolites were observed (Prakash et al., 2019), of which M1, M3, and M4 appeared to be similar to the in vitro experiments based on fragmentation patterns. Metabolites M5 and M6 were not detected in human plasma samples.

Later studies have shown that CYP3A4 is a major enzyme, and concomitant use of moderate and strong CYP3A4 inhibitors or strong CYP3A4 inducers may affect ivosidenib exposure (Fan et al., 2020a; Jiang et al., 2021). This is in agreement with the study in healthy participants where coadministration of the strong CYP3A4 inhibitor itraconazole increased ivosidenib exposure (Dai et al., 2019). However, concomitant administration of weak CYP3A4 inhibitors/inducers does not appear to affect ivosidenib CL in patients with m*IDH1* malignancies (Fan et al., 2020a). The impact of ivosidenib as an inhibitor or inducer of CYP enzymes was found to be manageable. CYP inhibition IC_{50} was >50 µM for all CYP enzymes assessed and there was no time- or metabolism-dependent inhibition of CYP enzymes, suggesting that formation of reactive metabolites is unlikely. Hence, the risk of serious drug-drug interactions caused by competitive or mechanism-based inhibition of CYP enzymes at the projected total exposure of 2.59 µM is considered to be low. Moderate induction of CYP3A4 and CYP2B6 was observed in vitro. The CYP3A4 induction potential of ivosidenib was further confirmed in a clinical study based on endogenous biomarker 4β-hydroxycholesterol/cholesterol ratios (Fan et al., 2020a). Concomitant use of ivosidenib with sensitive CYP3A4 substrate drugs should be avoided or patients monitored for loss of therapeutic effect if this is unavoidable (Agios Pharmaceuticals Inc., 2019).

The risk of autoinduction was considered to be low based on in vitro assessment in human hepatocyte cultures. However, an observed increase in apparent CL after multiple dosing in patients may be partly attributed to moderate autoinduction of ivosidenib metabolism (Fan et al., 2020a).

In vitro experiments have indicated that ivosidenib has high cell membrane permeability and appears to be a substrate of P-gp but not BCRP. As a substrate of P-gp, concomitant medications that inhibit P-gp may increase the exposure of ivosidenib, as demonstrated with the P-gp inhibitor itraconazole, in healthy participants (Dai et al., 2019).

There was a clear PK/PD relationship in the mouse HT1080 tumor xenograft model: plasma and tumor 2-HG concentrations decreased rapidly following administration of ivosidenib, and inhibition was dose and exposure dependent. The PK/PD relationship established in the xenograft mouse model is consistent with in vitro potency assessments (Popovici-Muller et al., 2018) and in clinical trials of patients with m*IDH1* advanced solid and hematologic malignancies (Fan et al., 2020a). In these patients, multiple doses of ivosidenib were associated with reductions in plasma 2-HG concentrations to levels similar to those observed in healthy participants (up to 98% reduction), with tumor and bone marrow 2-HG concentrations correlating positively with plasma 2-HG (Fan et al., 2020a). Ivosidenib trough concentration (C_{trough}) at 500 mg QD doses was 4975 ng/mL and higher than mouse IC_{97} (1075 ng/mL) even after accounting for PPB differences between mouse and human plasma (Fan et al., 2020a).

Based on the projected parameters, the preliminary efficacious dose in humans was projected to be in the range of 760–1080 mg administered orally b.i.d. However, clinical evidence continues to support the use of the approved 500 mg q.d. dosing regimen (DiNardo et al., 2018; Abou-Alfa et al., 2020; Fan et al., 2020a; Mellinghoff et al., 2020; Tap et al., 2020) and particularly the robust, persistent, maximal 2-HG reduction observed with this regimen in patients with advanced solid and hematologic cancers (Fan et al., 2020a). The higher projected dose compared with the approved dose may be attributed in part to the clinical dose being determined by the conservative CL projection, potential bioavailability differences, and clinical efficacy endpoint, instead of PKPD relationships.

In conclusion, the findings presented here extend our knowledge of the preclinical ADME and PK/PD profile of ivosidenib generated during the developability assessment of the molecule, supported its continued development in humans, and are fairly predictive of the profile seen clinically in patients with advanced m*IDH1* hematologic and solid tumors.

Acknowledgments

Medical writing assistance was provided by Shirley Louise-May of Excel Medical Affairs, Fairfield, CT, and supported by Agios Pharmaceuticals, Inc. and Servier Pharmaceuticals LLC.

DMD Fast Forward. Published on July 28, 2021 as DOI: 10.1124/dmd.120.000234
This article has not been copyedited and formatted. The final version may differ from this version.

Authorship Contributions

Participated in research design: Chen, Fan, Utley, Lemieux, Popovici-Muller, Dang, Su, Biller, Yang.

Conducted experiments: Chen, Utley, Kim, Yan, Yang.

Contributed new reagents or analytic tools: Lemieux, Popovici-Muller, Dang.

Performed data analysis: Chen, Nagaraja, Fan, Utley, Kim, Yan, Yang.

Wrote or contributed to the writing of the manuscript: Chen, Nagaraja, Fan, Utley, Lemieux, Popovici-Muller, Dang, Kim, Yan, Su, Biller, Yang.

References

Abou-Alfa GK, Macarulla T, Javle MM, Kelley RK, Lubner SJ, Adeva J, Cleary JM, Catenacci DV, Borad MJ, Bridgewater J, Harris WP, Murphy AG, Oh DY, Whisenant J, Lowery MA, Goyal L, Shroff RT, El-Khoueiry AB, Fan B, Wu B, Chamberlain CX, Jiang L, Gliser C, Pandya SS, Valle JW, and Zhu AX (2020) Ivosidenib in IDH1-mutant, chemotherapy-refractory cholangiocarcinoma (ClarIDHy): a multicentre, randomised, double-blind, placebo-controlled, phase 3 study. *Lancet Oncol* **21:**796-807.

Agios Pharmaceuticals Inc. (2019) *TIBSOVO (ivosidenib) highlights of prescribing information*, Agios Pharmaceuticals, Inc. Accessed July 13, 2020. https://www.accessdata.fda.gov/drugsatfda_docs/label/2019/211192s001lbl.pdf.

Bjornsson TD, Callaghan JT, Einolf HJ, Fischer V, Gan L, Grimm S, Kao J, King SP, Miwa G, Ni L, Kumar G, McLeod J, Obach RS, Roberts S, Roe A, Shah A, Snikeris F, Sullivan JT, Tweedie D, Vega JM, Walsh J, and Wrighton SA; Pharmaceutical Research and Manufacturers of America (PhRMA) Drug Metabolism/Clinical Pharmacology Technical Working Group; FDA Center for Drug Evaluation and Research (CDER) (2003) The conduct of in vitro and in vivo drug-drug interaction studies: a Pharmaceutical Research and Manufacturers of America (PhRMA) perspective. *Drug Metab Dispos* **31:**815–832.

Dai D, Yang H, Nabhan S, Liu H, Hickman D, Liu G, Zacher J, Vutikullird A, Prakash C, Agresta S, Bowden C, and Fan B (2019) Effect of itraconazole, food, and ethnic origin on the pharmacokinetics of ivosidenib in healthy subjects. *Eur J Clin Pharmacol* **75:**1099–1108.

Dang L, White DW, Gross S, Bennett BD, Bittinger MA, Driggers EM, Fantin VR, Jang HG, Jin S, Keenan MC, Marks KM, Prins RM, Ward PS, Yen KE, Liau LM, Rabinowitz JD, Cantley LC, Thompson CB, Vander Heiden MG, and Su SM (2009) Cancer-associated IDH1 mutations produce 2-hydroxyglutarate. *Nature* **462:**739–744.

Davies B and Morris T (1993) Physiological parameters in laboratory animals and humans. *Pharm Res* **10:**1093-1095.

DiNardo CD, Stein EM, de Botton S, Roboz GJ, Altman JK, Mims AS, Swords R, Collins RH, Mannis GN, Pollyea DA, Donnellan W, Fathi AT, Pigneux A, Erba HP, Prince GT, Stein AS, Uy GL, Foran JM, Traer E, Stuart RK, Arellano ML, Slack JL, Sekeres MA, Willekens C, Choe S, Wang H, Zhang V, Yen KE, Kapsalis SM, Yang H, Dai D, Fan B, Goldwasser M, Liu H, Agresta S, Wu B, Attar EC, Tallman MS, Stone RM, and Kantarjian HM (2018) Durable remissions with ivosidenib in IDH1-mutated relapsed or refractory AML. *N Engl J Med* **378:**2386–2398.

Fan B, Dai D, Cohen M, Xu H, Yin F, Nagaraja R, Mobilia M, Almon C, Basile FG, and Yang H (2021) Effect of mild and moderate hepatic impairment on the pharmacokinetics, safety, and tolerability of a single dose of oral ivosidenib in otherwise healthy participants. *Clin Pharmacol Drug Dev* **10:**99-109.

Fan B, Dai D, DiNardo CD, Stein E, de Botton S, Attar EC, Liu H, Liu G, Lemieux I, Agresta SV, and Yang H (2020a) Clinical pharmacokinetics and pharmacodynamics of ivosidenib in patients with advanced hematologic malignancies with an IDH1 mutation. *Cancer Chemother Pharmacol* **85:**959–968.

Fan B, Mellinghoff IK, Wen PY, Lowery MA, Goyal L, Tap WD, Pandya SS, Manyak E, Jiang L, Liu G, Nimkar T, Gliser C, Prahl Judge M, Agresta S, Yang H, and Dai D (2020b) Clinical pharmacokinetics and pharmacodynamics of ivosidenib, an oral, targeted inhibitor of mutant IDH1, in patients with advanced solid tumors. *Invest New Drugs* **38:**433–444.

Huang SM, Strong JM, Zhang L, Reynolds KS, Nallani S, Temple R, Abraham S, Habet SA, Baweja RK, Burckart GJ, Chung S, Colangelo P, Frucht D, Green MD, Hepp P, Karnaukhova E, Ko HS, Lee JI, Marroum PJ, Norden JM, Qiu W, Rahman A, Sobel S, Stifano T, Thummel K, Wei XX, Yasuda S, Zheng JH, Zhao H, and Lesko LJ (2008) New era in drug interaction evaluation: US Food and Drug Administration update on CYP enzymes, transporters, and the guidance process. *J Clin Pharmacol* **48:**662–670.

Iwatsubo T, Suzuki H, and Sugiyama Y (1997) Prediction of species differences (rats, dogs, humans) in the in vivo metabolic clearance of YM796 by the liver from in vitro data. *J Pharmacol Exp Ther* **283:**462-469.

Jiang X, Wada R, Poland B, Kleijn HJ, Fan B, Liu G, Liu H, Kapsalis S, Yang H, and Le K (2021) Population pharmacokinetic and exposure-response analyses of ivosidenib in patients with *IDH1*-mutant advanced hematologic malignancies. *Clin Transl Sci***:**Online ahead of print.

Lu C, Ward PS, Kapoor GS, Rohle D, Turcan S, Abdel-Wahab O, Edwards CR, Khanin R, Figueroa ME, Melnick A, Wellen KE, O'Rourke DM, Berger SL, Chan TA, Levine RL, Mellinghoff IK, and Thompson CB (2012) IDH mutation impairs histone demethylation and results in a block to cell differentiation. *Nature* **483:**474–478.

Mellinghoff IK, Cloughesy TF, Wen PY, Taylor JW, Maher EA, Arrillaga-Romany I, Peters KB, Choi C, Ellingson BM, Lin AP, Thakur SB, Nicolay B, Lu M, Le K, Yin F, Tai F, Schoenfeld S, Pandya SS, Hassan I, Steelman L, and Clarke J (2019) A phase 1, open-label, perioperative study of ivosidenib (AG-120) and vorasidenib (AG-881) in recurrent, IDH1-mutant, low-grade glioma: updated results. *ACTR-66 presented at the 24th Annual Scientific Meeting and Education Day of the Society for Neuro-Oncology (SNO), Nov 22–24, 2019, Phoenix, Arizona, USA*.

Mellinghoff IK, Ellingson BM, Touat M, Maher E, De La Fuente MI, Holdhoff M, Cote GM, Burris H, Janku F, Young RJ, Huang R, Jiang L, Choe S, Fan B, Yen K, Lu M, Bowden C, Steelman L, Pandya SS, Cloughesy TF, and Wen PY (2020) Ivosidenib in isocitrate dehydrogenase 1-mutated advanced glioma. *J Clin Oncol* **38:**3398-3406.

Nicolay B, Narayanaswamy R, Aguado E, Nagaraja R, Murtie J, Liu G, and Ishii Y (2017) The IDH1 mutant inhibitor AG-120 shows strong inhibition of 2-HG production in an orthotopic IDH1 mutant glioma model *in vivo*. *Poster EXTH-59 presented at the 22nd Annual Scientific Meeting and Education Day of the Society for Neuro-oncology, November 16–19, 2017, San Francisco, CA, USA*.

Obach RS (2000) Metabolism of ezlopitant, a nonpeptidic substance P receptor antagonist, in liver microsomes: enzyme kinetics, cytochrome P450 isoform identity, and in vitro-in vivo correlation. *Drug Metab Dispos* **28:**1069-1076.

Obach RS, Baxter JG, Liston TE, Silber BM, Jones BC, MacIntyre F, Rance DJ, and Wastall P (1997) The prediction of human pharmacokinetic parameters from preclinical and in vitro metabolism data. *J Pharmacol Exp Ther* **283:**46-58.

Ogilvie BW, Usuki E, Yerino P, and Parkinson A (2008) In vitro approaches for studying the inhibition of drug-metabolizing enzymes and identifying the drug-metabolizing enzymes responsible for the metabolism of drugs (reaction phenotyping) with emphasis on cytochrome P450, in *Drug-Drug Interactions* (Rodrigues DA ed) pp 231–358, Informa Healthcare, New York.

Oie S and Tozer TN (1979) Effect of altered plasma protein binding on apparent volume of distribution. *J Pharm Sci* **68:**1203-1205.

Popovici-Muller J, Lemieux RM, Artin E, Saunders JO, Salituro FG, Travins J, Cianchetta G, Cai Z, Zhou D, Cui D, Chen P, Straley K, Tobin E, Wang F, David MD, Penard-Lacronique V, Quivoron C, Saada V, de Botton S, Gross S, Dang L, Yang H, Utley L, Chen Y, Kim H, Jin S, Gu Z, Yao G, Luo Z, Lv X, Fang C, Yan L, Olaharski A, Silverman L, Biller S, Su SM, and Yen K (2018) Discovery of AG-120 (ivosidenib): a first-in-class mutant IDH1 inhibitor for the treatment of IDH1 mutant cancers. *ACS Med Chem Lett* **9:**300–305.

Prakash C, Fan B, Altaf S, Agresta S, Liu H, and Yang H (2019) Pharmacokinetics, absorption, metabolism, and excretion of [(14)C]ivosidenib (AG-120) in healthy male subjects. *Cancer Chemother Pharmacol* **83:**837–848.

Saha SK, Parachoniak CA, Ghanta KS, Fitamant J, Ross KN, Najem MS, Gurumurthy S, Akbay EA, Sia D, Cornella H, Miltiadous O, Walesky C, Deshpande V, Zhu AX, Hezel AF, Yen KE, Straley KS, Travins J, Popovici-Muller J, Gliser C, Ferrone CR, Apte U, Llovet JM, Wong KK, Ramaswamy S, and Bardeesy N (2014) Mutant IDH inhibits HNF-4α to block hepatocyte differentiation and promote biliary cancer. *Nature* **513:**110–114.

Tap WD, Villalobos VM, Cote GM, Burris H, Janku F, Mir O, Beeram M, Wagner AJ, Jiang L, Wu B, Choe S, Yen K, Gliser C, Fan B, Agresta S, Pandya SS, and Trent JC (2020) Phase I Study of the Mutant IDH1 Inhibitor Ivosidenib: Safety and Clinical Activity in Patients With Advanced Chondrosarcoma. *J Clin Oncol* **38:**1693-1701.

U.S. Department of Health and Human Services Food and Drug Administration (2012) *Draft Guidance for Industry: Drug Interaction Studies—Study Design, Data Analysis, Implications for Dosing, and Labeling Recommendations*, U.S. Department of Health and Human Services, Rockville, MD.

Ward PS, Patel J, Wise DR, Abdel-Wahab O, Bennett BD, Coller HA, Cross JR, Fantin VR, Hedvat CV, Perl AE, Rabinowitz JD, Carroll M, Su SM, Sharp KA, Levine RL, and Thompson CB (2010) The common feature of leukemia-associated IDH1 and IDH2 mutations is a neomorphic enzyme activity converting alpha-ketoglutarate to 2-hydroxyglutarate. *Cancer Cell* **17:**225–234.

Xu W, Yang H, Liu Y, Yang Y, Wang P, Kim SH, Ito S, Yang C, Wang P, Xiao MT, Liu LX, Jiang WQ, Liu J, Zhang JY, Wang B, Frye S, Zhang Y, Xu YH, Lei QY, Guan KL, Zhao SM, and Xiong Y (2011) Oncometabolite 2-hydroxyglutarate is a competitive inhibitor of α-ketoglutarate-dependent dioxygenases. *Cancer Cell* **19:**17–30.

Yen K, Lemieux R, Popovici-Muller J, Chen Y, Yang H, Straley K, Choe S, Dorsch M, Agresta S, Schenkein DP, Biller S, Su M, and Wang F (2013) IDH1 mutant inhibitor induces cellular differentiation and offers a combination benefit with Ara-C in a primary human Idh1 mutant AML xenograft model. *Blood* **122:**3946.

Footnotes

Funding

This work was supported by Agios Pharmaceuticals, Inc.

Conflict of Interest and Financial Disclosures

Y.C., L.D., H.K., and S.A.B.: employee and stock-holder of Agios Pharmaceuticals, Inc. N.V.N. was an employee and stock-holder of Agios Pharmaceuticals, Inc. at the time of submission of this work and is currently an employee of Servier Pharmaceuticals LLC. B.F., L.U., R.M.L., J.P.-M., S.-S.M.S., and H.Y.: employee and stock-holder of Agios Pharmaceuticals, Inc. at the time of this work. L.Y.: employee of ChemPartner, a vendor contracted to perform research for Agios Pharmaceuticals, Inc.

Legends for Figures

Fig. 1. Single-dose pharmacokinetic profiles of ivosidenib following (A) intravenous (i.v.) and (B) p.o. administration in rats, dogs, and monkeys.

Fig. 2. Tentative structures of ivosidenib metabolites formed in rat, dog, monkey, and human liver microsomes.

Fig. 3. Mean ± S.D. ivosidenib and D-2-hydroxyglutarate (2-HG) concentrations following repeated (20, 50, and 150 mg/kg b.i.d.) oral dosing of ivosidenib in the HT1080 mouse xenograft tumor model. Horizontal dotted line shows baseline 2-HG levels. PK, pharmacokinetic; PK/PD, pharmacokinetic-pharmacodynamic relationship.

Fig. 4. Ivosidenib $AUC_{0–12h}$ versus 2-HG C_{avg} in a 12-hour interval following multiple oral dosing of ivosidenib (20 to 150 mg/kg) in a mouse HT1080 xenograft model. $AUC_{0–12h}$, area under the curve from 0 to 12 hours; C_{avg}, average plasma concentration.

Tables

TABLE 1

Single-dose pharmacokinetic parameters of ivosidenib following i.v. and p.o. administration in rats, dogs, and monkeys, mean (S.D.)

Pharmacokinetic Parameters After Single Ivosidenib Dose	Rat		Dog		Monkey	
	i.v. (1 mg/kg)	p.o. (10 mg/kg)	i.v. (1 mg/kg)	p.o. (10 mg/kg)	i.v. (1 mg/kg)	p.o. (10 mg/kg)
T_{max}, h	NA	2.7 (1.2)	0.14 (0.05)	9.5 (12.7)	0.22 (0.05)	5.3 (2.3)
C_{max}, ng/ml	NA	2373 (457)	7986 (5423)	3707 (2846)	1001 (255)	1681 (446)
$AUC_{0–12h}$, ng•h/ml	3183 (661)	16,852 (1260)	16,384 (11,707)	36,307 (30,121)	3878 (469)	15,539 (3359)
$AUC_{0–24h}$, ng•h/ml	4469 (1103)	21,115 (1384)	28,889 (20,792)	74,733 (59,211)	4901 (436)	24,020 (4246)
$AUC_{0–inf}$, ng•h/ml	5372 (2053)	21,195 (1412)	56,017 (41,326)		5091 (345)	27,404 (4439)
$t_{½}$, h	8.9 (3.7)	2.9 (0.2)	18.5 (2.1)		5.3 (0.88)	8.0 (0.8)
CL, l/h/kg	0.20 (0.73)		0.024 (0.014)		0.197 (0.014)	
CL_r, l/h/kg	0.003 (0.002)		0.0003 (0.0002)		0.001 (0.0006)	
V_{ss}, l/kg	2.10 (0.28)		0.73 (0.43)		1.24 (0.32)	

F, %	39.5 (2.6)	25.9 (20.5)	53.8 (8.7)

$AUC_{0–12h}$, area under the concentration-time curve from time 0 to 12 hours postdose; $AUC_{0–24h}$, area under the concentration-time curve from time 0 to 24 hours postdose; $AUC_{0–inf}$, area under the concentration-time curve extrapolated to infinity; CL, clearance; CL_r, renal clearance; C_{max}, maximum plasma concentration; F, bioavailability; i.v., intravenous; NA, not applicable; $t_{½}$, elimination half-life; T_{max}, time to maximum concentration; V_{ss}, volume at steady state.

TABLE 2

In vitro evaluation of ivosidenib as an inhibitor of human CYP enzymes

Enzyme	Enzyme reaction	Direct inhibition, zero-minute preincubation		Time-dependent inhibition, 30-minute preincubation without NADPH		Metabolism-dependent inhibition, 30-minute preincubation with NADPH	
		IC_{50} (µM)[a]	Inhibition observed at 50 µM (%)[b]	IC_{50} (µM)[a]	Inhibition observed at 50 µM (%)[b]	IC_{50} (µM)[a]	Inhibition observed at 50 µM (%)[b]
CYP1A2	Phenacetin O-dealkylation	> 50	3.9	> 50	3.7	> 50	4.0
CYP2B6	Efavirenz 8-hydroxylation	> 50	5.3	> 50	8.6	> 50	6.2
CYP2C8	Amodiaquine N-dealkylation	> 50	44	> 50	46	> 50	48
CYP2C9	Diclofenac 4′-hydroxylation	> 50	17	> 50	17	> 50	22
CYP2C19	S-mephenytoin 4′-hydroxylation	> 50	31	> 50	31	> 50	28
CYP2D6	Dextromethorphan O-demethylation	> 50	44	> 50	46	> 50	45
CYP3A4/5	Testosterone 6β-hydroxylation	> 50	33	> 50	20	> 50	44
CYP3A4/5	Midazolam 1′-hydroxylation	> 50	48	> 50	46	47	53

CYP, cytochrome P450; NADPH, nicotinamide adenine dinucleotide phosphate.

[a] Average data from duplicate samples.

[b] Inhibition observed (%) is calculated as (100% - percent solvent control).

TABLE 3

CYP enzyme induction as measured by marker substrate activity after treatment with 0.1–90 µM ivosidenib

CYP	CYP1A2			CYP2B6			CYP3A4/5		
Hepatocyte donor	HC3-15	HC3-18	HC5-25	HC3-15	HC3-18	HC5-25	HC3-15	HC3-18	HC5-25
Activity E_{max}, fold increase	4.99^{a}	NT	NT	8.04^{b}	3.18^{a}	NT	3.53^{a}	NT	2.47^{a}
Activity EC_{50}, µM	53.4^{a}	NC	NC	2.45^{b}	1.00^{a}	NT	1.06^{a}	NC	0.631^{a}
mRNA E_{max}, fold increase	2.83^{a}	2.09^{a}	NC	4.45^{b}	2.69^{a}	1.40^{a}	208^{a}	21.7^{a}	4.99^{a}
mRNA EC_{50}, µM	37.9^{a}	72.2^{a}	NC	3.33^{b}	2.18^{a}	3.29^{a}	22.9^{a}	9.39^{a}	5.27^{a}

CYP, cytochrome P450; EC_{50}, half-maximal effective concentration; E_{max}, maximum effect; NC, not calculated (fold change <2); NT, not tested.

[a] Based on the enzyme activity concentration-response curves, using sigmoidal three-parameter fit.

[b] Based on the enzyme activity concentration-response curves, using sigmoidal Hill three-parameter fit.

TABLE 4

The effects of autoinduction with ivosidenib on CYP enzymes as measured by the clearance of deuterated analog of ivosidenib (AGI-18070) in hepatocytes from three different donors

Treatment	Concentration	Intrinsic Clearance (µL/min/million cells)					
		0.1 µM AGI-18070			1 µM AGI-18070		
		HC3-15	HC3-18	HC5-25	HC3-15	HC3-18	HC5-25
Dimethyl sulfoxide	0.1% (v/v)	2.29	2.71	2.12	2.92	4.17	3.85
Ivosidenib	1 µM	1.88	2.50	3.08	2.92	4.17	4.04
Ivosidenib	10 µM	4.38	2.71	3.08	2.71	3.75	4.42
Ivosidenib	50 µM	1.88	2.92	2.88	2.92	3.54	3.65
Ivosidenib	90 µM	2.29	2.71	3.08	2.92	3.54	3.85
Rifampin	10 µM	2.08	2.71	4.42	2.92	3.75	4.81

CYP, cytochrome P450.

In vitro intrinsic clearance (µL/min/million cells protein) {exponential decay} = (0.693 ÷ half-life (min) {exponential decay}) x incubation volume (µL) ÷ protein per incubation (million cells/inc).

TABLE 5

Bidirectional permeability of $[^{14}C]$-ivosidenib (5 μM) across MDCKII-P-gp and control cells in the presence of valspodar and verapamil

Substrate	Inhibitor	[Inhibitor], μM	Control: $P_{app} \times 10^{-6}$ cm/s, mean ± S.D. Apical to Basal	Control: $P_{app} \times 10^{-6}$ cm/s, mean ± S.D. Basal to Apical	Control: Efflux Ratio	P-gp: $P_{app} \times 10^{-6}$ cm/s, mean ± S.D. Apical to Basal	P-gp: $P_{app} \times 10^{-6}$ cm/s, mean ± S.D. Basal to Apical	P-gp: Efflux Ratio	Net Efflux Ratio	Relative Transport (Percent of Control), %
$[^{14}C]$-ivosidenib	NA	0	39.4 ± 7.2	66.8 ± 7.1	1.69	5.67 ± 3.61	119 ± 3	21.0	12.4	100
	Verapamil	60	53.0 ± 4.5	54.5 ± 0.5	1.03	38.3 ± 11.9	69.2 ± 0.8	1.80	1.75	6.6
	Valspodar	10	46.3 ± 4.3	43.9 ± 4.4	0.950	25.5 (*n* = 2)	41.5 ± 4.5	1.63	1.72	6.3
Digoxin	NA	0	2.78 ± 0.40	10.4 ± 0.7	3.75	0.549 ± 0.053	23.3 ± 0.5	42.4	11.3	100
	Verapamil	60	6.01 ± 0.59	6.61 (*n* = 2)	1.10	3.92 ± 0.02	7.87 ± 0.36	2.01	1.82	8.0
	Valspodar	10	4.30 ± 0.59	5.95 (*n* = 2)	1.38	3.45 ± 0.84	4.74 ± 0.44	1.38	0.994	-0.1

MDCKII, Madin-Darby Canine Kidney II; NA, not applicable; P_{app}, apparent permeability; P-gp, P-glycoprotein.

Values are triplicate determinations rounded to three significant figures with S.D. rounded to the same degree of accuracy. Percentages are rounded to one decimal place except percentages ≥100, which are rounded to the nearest whole number.

TABLE 6

Bidirectional permeability of [^{14}C]-ivosidenib (5 µM) across MDCKII-BCRP and control cells in the presence of BCRP inhibitor Ko143

Substrate	Inhibitor	[Inhibitor], µM	Control: P_{app}, × 10^{-6} cm/s, Apical to Basal	Control: P_{app}, × 10^{-6} cm/s, Basal to Apical	Control: Efflux Ratio	BCRP: P_{app}, × 10^{-6} cm/s, Apical to Basal	BCRP: P_{app}, × 10^{-6} cm/s, Basal to Apical	BCRP: Efflux Ratio	Net Efflux Ratio	Relative Transport (Percent of Control), %
[^{14}C]-ivosidenib	Ko143	0	34.7 ± 4.0	43.3 ± 16.6	1.25	43.5 (*n* = 2)	32.0 ± 5.0	0.737	0.590	NA
		1	23.6 ± 11.7	47.7 ± 9.3	2.02	18.5 (*n* = 2)	32.1 ± 4.2	1.74	0.859	NA
Prazosin	Ko143	0	21.4 ± 7.4	34.4 ± 9.0	1.61	11.3 (*n* = 2)	60.0 (*n* = 2)	5.31	3.31	100
		1	20.3 ± 7.9	32.2 ± 5.7	1.59	33.0 (*n* = 2)	32.8 (*n* = 2)	0.995	0.626	−16.2

BCRP, breast cancer resistance protein; MDCKII, Madin-Darby Canine Kidney II; NA, not applicable; P_{app}, apparent permeability.

Values are triplicate determinations rounded to three significant figures, with S.D. rounded to the same degree of accuracy. Percentages are rounded to one decimal place except percentages ≥100, which are rounded to the nearest whole number.

TABLE 7

PK/PD profile of ivosidenib in HT1080 tumor xenograft mouse model after three b.i.d. doses

Group	Ivosidenib $AUC_{0–12h}$, h•ng/mL	2-HG $AUC_{0–12h}$, h•ng/g	2-HG $C_{average}$, mM	Reduction of 2-HG Based on $AUC_{0–12h}$, %	Maximal Reduction of 2-HG, %	Reduction of 2-HG at 12 h
	Plasma	Tumor	Tumor	Tumor	Tumor	Tumor
Vehicle	NA	11865872	6.77	NA	NA	NA
20 mg/kg, 3 doses	5129	1378257	0.79	87.8	93.3	88.3
50 mg/kg, 3 doses	13058	559876	0.32	95.0	97.2	94.2
150 mg/kg, 3 doses	29196	71318	0.041	99.4	99.7	99.0

2-HG, D-2-hydroxyglutarate; $AUC_{0–12h}$, area under the concentration-time curve from time 0 to 12 hours; $C_{average}$, average concentration; NA, not applicable.

TABLE 8

PK/PD parameters for ivosidenib in the HT1080 tumor xenograft mouse model after three b.i.d. doses

Parameter	Estimate
E0	6.78 mM
$EAUC_{50}$(0–12h)	398 h•ng/ml
$EAUC_{90}$(0–12h)	3600 h•ng/ml
$EAUC_{97}$(0–12h)	12900 h•ng/ml

E0, baseline effect, corresponding to response when dose of drug is zero; EAUC, efficacious area under the curve; $EAUC_{50/90/97}$(0–12h), EAUC from 0–12h resulting in 50/90/97% tumor 2-HG inhibition.

Figures

Fig. 1.

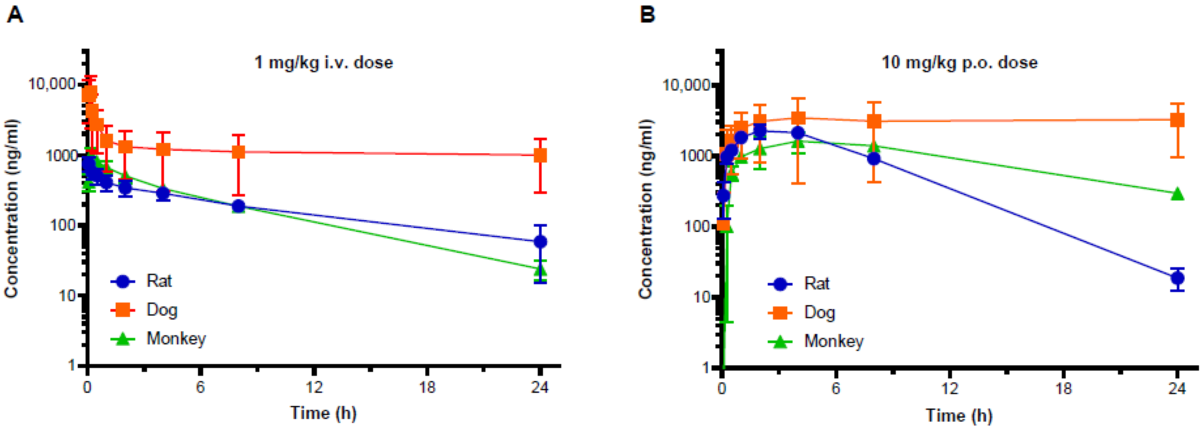

DMD Fast Forward. Published on July 28, 2021 as DOI: 10.1124/dmd.120.000234
This article has not been copyedited and formatted. The final version may differ from this version.

Fig. 2.

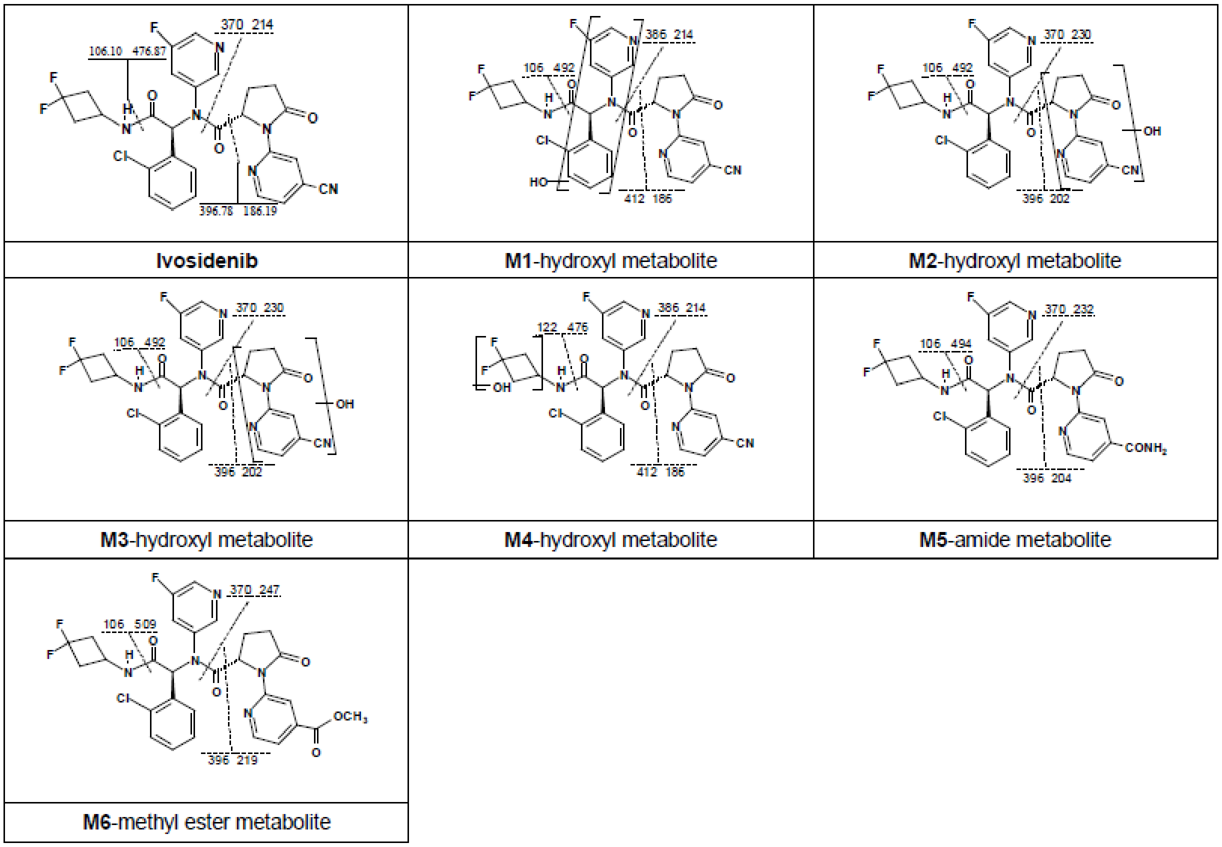
370 214
106.10 476.87
396.78 186.19
F
F
F
H
N
O
N
O
N
O
Cl
N
CN
Ivosidenib
386 214
106 492
412 186
HO
M1-hydroxyl metabolite
370 230
106 492
396 202
OH
M2-hydroxyl metabolite
370 230
106 492
396 202
OH
M3-hydroxyl metabolite
386 214
122 476
412 186
OH
M4-hydroxyl metabolite
370 232
106 494
396 204
CONH₂
M5-amide metabolite
370 247
106 509
396 219
OCH₃
M6-methyl ester metabolite

DMD Fast Forward. Published on July 28, 2021 as DOI: 10.1124/dmd.120.000234
This article has not been copyedited and formatted. The final version may differ from this version.

Fig. 3.

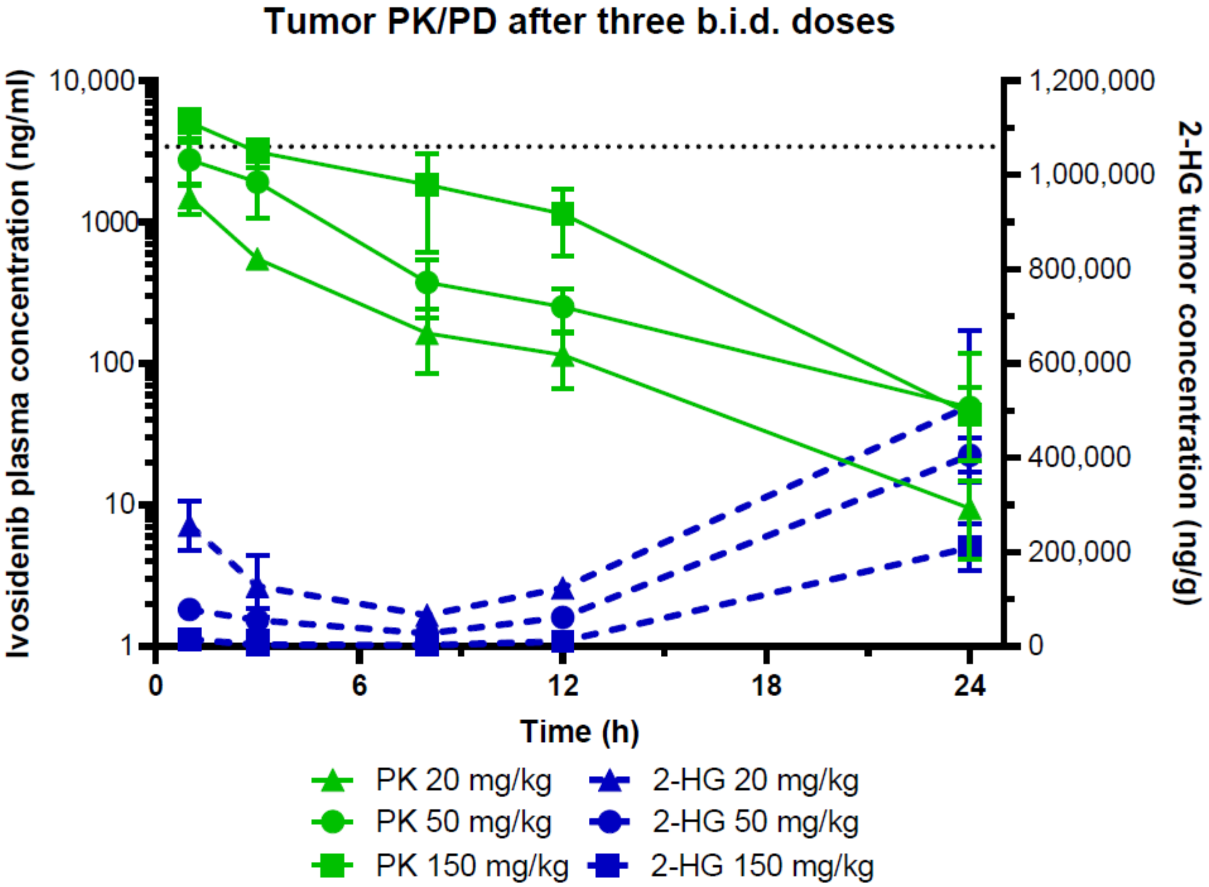

DMD Fast Forward. Published on July 28, 2021 as DOI: 10.1124/dmd.120.000234
This article has not been copyedited and formatted. The final version may differ from this version.

Fig. 4.

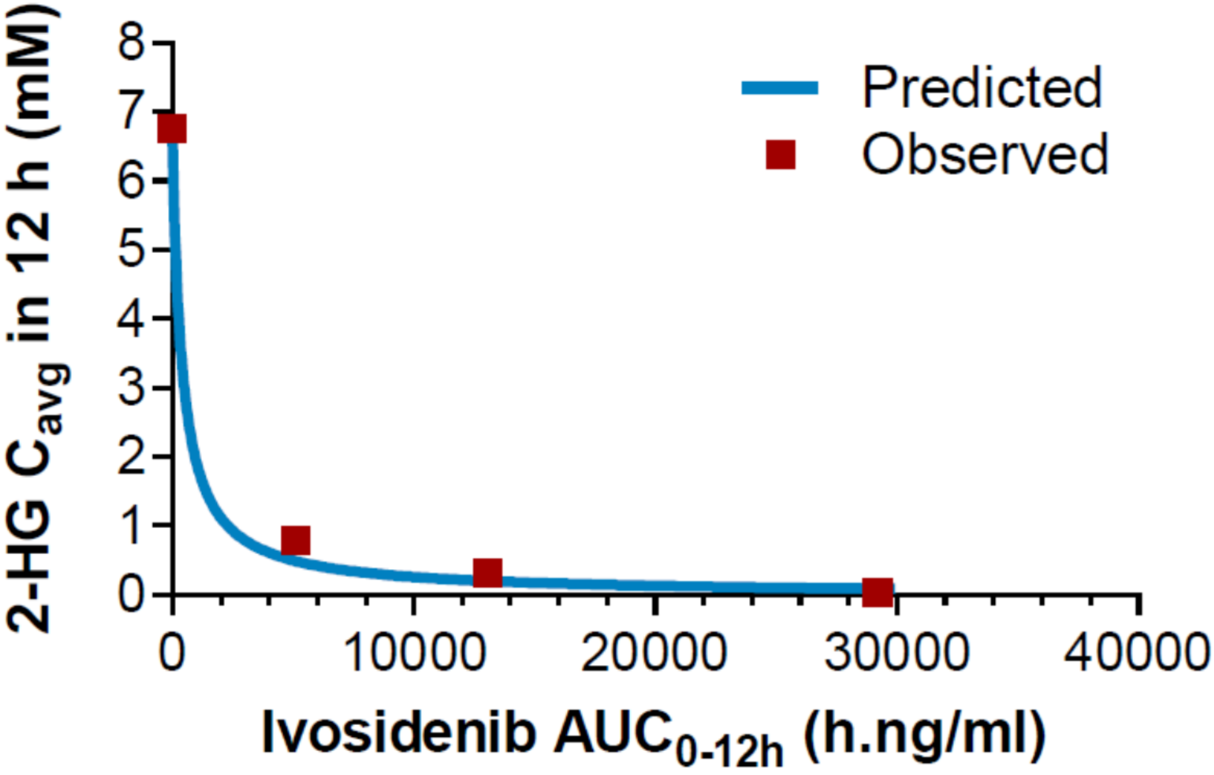
2-HG C_{avg} in 12 h (mM)
8
7
6
5
4
3
2
1
0
0
10000
20000
30000
40000
Ivosidenib AUC_{0-12h} (h.ng/ml)
Predicted
Observed